Multifragmentation within a clusterization algorithm based on thermal binding energies

Rohit Kumar,[1] Sakshi Gautam,[2,*] and Rajeev K. Puri[1]
[1]*Department of Physics, Panjab University, Chandigarh 160 014, India*
[2]*Department of Physics, Dev Samaj College for Women, Sector 45 B, Chandigarh 160 047, India*
(Received 2 March 2014; revised manuscript received 4 April 2014; published 17 June 2014)

The formation of the fragments in a reaction is addressed by modifying the minimum spanning tree method by using thermal binding energies. Each fragment is subjected to the fulfillment of thermal binding energy. Our detailed investigation covering different masses, incident energies, and impact parameters indicates a significant role of thermal binding energies over that of cold matter.

DOI: 10.1103/PhysRevC.89.064608 PACS number(s): 25.70.Pq, 21.10.Dr, 24.10.Cn, 24.10.Lx

I. INTRODUCTION

The decay (or breakup) of excited nuclei into free nucleons and fragments of various sizes (known as "nuclear multifragmentation") is a fascinating process that occupies a central place and is a current topic in nuclear physics [1]. Several interesting aspects of multifragmentation as a function of incident energy [2], colliding geometry [3], as well as system size [4] have been measured experimentally and studied theoretically and have provided a unique opportunity to understand various questions such as the origin and time scale of fragmentation and the role of dynamical correlations in their formation. The large domain of incident energy and system masses allows one to also construct multifragmentation systematics.

The physics behind nuclear multifragmentation can be studied by using either statistical models or dynamical models such as quantum molecular dynamics (QMD) [5] and Boltzmann-Uehling-Uhlenbeck (BUU) [6] models. The statistical multifragmentation models [2,7] ignore the dynamical part and shed light on the final distribution only. One often uses information generated by a dynamical model within a statistical model to study fragmentation. For example, one uses the phase space generated by a BUU/QMD model and switches to a statistical model for determination of final distributions [2,8]. On the other hand, in a dynamical model, one starts from the initial well-separated target and projectile and follows the reaction till the end. Here, ideally speaking, one needs to follow the reaction till thousands of fm/c where matter will be cold enough. The Monte Carlo technique used in the simulations, however, does not allow one to follow the reaction so long. One is constrained to stop the reaction at around 200–300 fm/c and identify the fragments using cluster identifiers. Some recent studies employ de-excitation calculations using the GEMINI code [9,10] to further de-excite the fragments formed by the cluster identifiers via sequential decay. In either case, one has to construct reliable fragments. It should be kept in the mind that all dynamical models follow the time evolution of single nucleons only and none simulate the fragments directly. The most widely used algorithm to identify the fragments is based on the spatial correlations among nucleons and has been dubbed as the minimum spanning tree (MST) method [5]. Since the MST method is based on the spatial correlations only, the fragments thus formed can have nucleons with very high relative momenta that may not remain in the fragment after a while. At the later stages when matter is diluted, such a question does not arise. As a result, one has to be concerned with the nature of the fragments thus formed. In spite of all these limitations, the minimum spanning tree method remains the most popular one. Recently, methods based on the simulated annealing technique have also been developed [11,12], but, apart from being complicated, these methods rely on several parameters, which limits their utility. Alternatively, a number of attempts at improving the normal (conventional) MST method have been made [13–15]. As stated earlier, among these, an additional constraint in momentum space [13] as well as subjecting each fragment to either constant or realistic binding energy (derived from the Bethe-Weizsäcker mass formula) checks [16] are the most prominent ones. The binding energy cut has also exposed the improper (or loosely) bound fragments detected by the MST method [14,15]. The bottleneck in the above binding energy cut was the use of the binding energy of cold matter. If one uses the MST method to pre-sort the fragment structure (to be used in the statistical models/GEMINI calculations later on), one has to deal with excited fragments. On the other hand, if the MST method is used to identify the final fragments in a dynamical model, then one has to follow the reaction for quite a long time. Generally, one does not follow the reaction beyond 200–300 fm/c because this might add a spurious yield in the fragments owing to a stability problem.

At the same time, the vast and rich available literature on nuclear multifragmentation clearly suggests that the fragments at the freeze-out stage are not cold [17–19] and therefore are excited. A large number of efforts have been dedicated to find the true temperature of the fragments [10,17–19]. The temperature of the fragments has been measured (1) by using the double isotope ratios of the fragments emitted in the initial pre-equilibrium stage [18] and (2) by measuring the excitation and kinetic energies of the fragments [17]. For example, in Ref. [18], the ratios of the yields of tritium to deuterium and ^{4}He to ^{3}He are used as a thermometer to calculate the temperature. In all these studies the temperature of the fragments is reported to be in the range of a few MeV. Therefore, one is confronted immediately with few

*sakshigautm@gmail.com

basic questions: (a) how much thermal binding energies affect the formation of the fragments and (b) whether or not the binding energies of the fragments created by the MST method correspond to thermal binding energies. As discussed above, earlier cold matter binding energies were used which will be quite different than that of a thermal bath. By subjecting excited fragments to cold binding energy, one can eliminate many fragments those are not cold. Therefore, while filtering out the fragments generated using the MST approach, the binding energy of the hot nuclear matter should be considered. This binding energy is actually the binding energy of the cluster in its (cold) ground state plus the excitation energy of the cluster (due to its finite temperature). To analyze these questions, we follow the reactions within the QMD model and then create fragments with the MST method subjected to thermal binding energies. The paper is organized as follows: Section II deals with the details of the formalism, Sec. III presents the results, and Sec. IV provides a summary.

II. FORMALISM

A. Quantum molecular dynamics model

The *quantum molecular dynamics* [4,5,12–15] model is an n-body model used to simulate heavy-ion reactions on an event-by-event basis. The time evolution of the nucleons is determined by the real and imaginary parts of the transition matrix. This model gives a microscopic description of heavy-ion collisions at the nucleonic level and describes the reaction dynamics from the initially separated projectile and target up to the final freeze-out stage where matter is fragmented. Here each nucleon is represented by a Gaussian in momentum and coordinate space,

$$\psi_i(\vec{r},\vec{p}_i(t),\vec{r}_i(t)) = \frac{1}{(2\pi L)^{\frac{3}{4}}} e^{[\frac{i}{\hbar}\vec{p}_i(t)\cdot\vec{r} - \frac{(\vec{r}-\vec{r}_i(t))^2}{4L}]}. \tag{1}$$

The mean position $\vec{r}_i(t)$ and mean momentum $\vec{p}_i(t)$ of a nucleon are the two time-dependent parameters. The centers of these Gaussian wave packets propagate in coordinate and momentum space according to Hamilton's classical equations of motion:

$$\dot{\vec{r}}_i = \frac{\partial H}{\partial \vec{p}_i}, \quad \dot{\vec{p}}_i = -\frac{\partial H}{\partial \vec{r}_i}, \tag{2}$$

where H stands for the Hamiltonian, which is given by

$$H = \sum_i \frac{p_i^2}{2m_i} + V^{\rm tot}. \tag{3}$$

The total interaction potential $V^{\rm tot}$ thus reads as

$$V^{\rm tot} = \sum_{i<j} V_{ij} = \sum_{i<j} \left[V_{ij}^{\rm Loc} + V_{ij}^{\rm Coul} + V_{ij}^{\rm Yuk}\right], \tag{4}$$

where $V^{\rm Loc}$ is the local (two- and three-body) Skyrme-type interactions:

$$V^{\rm Loc} = \sum_{ij} V_{ij}^{\rm Loc} = \frac{1}{2!}\sum_{j;i\neq j} V_{ij}^{(2)} + \frac{1}{3!}\sum_{j,k;i\neq j\neq k} V_{ijk}^{(3)}. \tag{5}$$

Here $V_{ij}^{(2)}$ and $V_{ijk}^{(3)}$ represent two- and three-body interactions, respectively, which in the limit of nuclear matter reduces to

$$V^{\rm Loc} = \frac{A}{2}\left(\frac{\rho}{\rho_o}\right) + \frac{B}{G+1}\left(\frac{\rho}{\rho_o}\right)^G. \tag{6}$$

The above two parameters A and B are fixed so that the average binding energy at the normal nuclear matter density should be -15.76 MeV and the total energy should have a minimum at ρ_o whereas G decides the compressibility. The Yukawa and Coulomb potentials are given by

$$V_{ij}^{\rm Yuk} = t_3 \frac{\exp[-|(\vec{r}_i-\vec{r}_j)|/\mu]}{[|(\vec{r}_i-\vec{r}_j)|/\mu]}, \tag{7}$$

$$V_{ij}^{\rm Coul} = \frac{Z_i Z_j e^2}{|(\vec{r}_i-\vec{r}_j)|}. \tag{8}$$

Here $t_3 = -6.66$ MeV, $\mu = 1.5$ fm, and Z_i and Z_j denote the charges of the ith and jth baryon, respectively. During the propagation, two nucleons suffer collisions if the distance between their centroids, $|\vec{r}_i - \vec{r}_j|$, is less than $\sqrt{\sigma/\pi}$. The phase space of nucleons, thus generated, is stored at several time steps during the propagation. This will then be subjected to a clusterization algorithm.

B. Clusterization algorithm with thermal binding energies

As mentioned above, we start with the simple MST method. In this method, two nucleons share the same cluster if their centroids in coordinate space are closer than 4 fm, i.e., $|\vec{r}_i - \vec{r}_j| \leqslant 4$ fm. Here no binding energy check is imposed. The MST algorithm is now modified by demanding that each fragment (created in the MST method) fulfills the following binding energy criterion:

$$\zeta_i = \sum_{i=1}^{N^f}\left[\frac{(\vec{p}_i - \vec{p}_{cm})^2}{2m} + \sum_{i<j}^{N^f} V_{ij}\right] < E_{\rm bind}^{\rm thermal}. \tag{9}$$

In this equation, N^f is the number of nucleons in a fragment and $\vec{p}_{cm}$ is the center-of-mass momentum of that fragment. Any fragment failing to satisfy the above constraint is treated as a bundle of free nucleons. It is worth mentioning that past attempts were made either by having a constant binding energy or using the binding energy of cold matter. We here rather use a temperature-dependent binding energy cut to identify the fragments. Lots of studies have been reported in the literature that give mass formulas at finite temperatures (i.e., at nonzero excitation energies) by using information about the low-lying spectra of nuclei [20,21]. Such mass formulas provide a simple parametrization of the binding energy of a nucleus as a function of its temperature. Among these, we shall use the recent one proposed by Davidson *et al.* [20]. In this parametrization [20], the temperature-dependent binding energy $E_{\rm bind}^{\rm thermal}$ reads as

$$E_{\rm bind}^{\rm thermal}(T) = \alpha(T)N_f + \beta(T)N_f^{2/3} + \left(\gamma(T) - \frac{\eta(T)}{{N_f}^{1/3}}\right)\left(\frac{4{t_\varsigma}^2 + 4|t_\varsigma|}{N_f}\right)$$

$$+0.8076\frac{{Z_f}^2 R(0)}{{N_f}^{1/3}R(T)}\left(1-\frac{0.7636}{{Z_f}^{2/3}}\right.$$
$$\left.-\ 2.29\frac{R(0)^2}{[R(T){N_f}^{1/3}]^2}\right)+\delta(T)\frac{f(N_f,Z_f)}{{N_f}^{3/4}}, \quad (10)$$

where N_f is the size of the fragment, Z_f is the effective charge of the fragment, and t_z represents the isospin asymmetry of the fragment. The values of the temperature-dependent parameters $\alpha(T)$, $\beta(T)$, $\gamma(T)$, $\delta(T)$, $\eta(T)$, and $R(T)$ are extracted from the graphical representation as given in Ref. [20]. When one uses $T = 0$ MeV, one gets the binding energy of cold matter (labeled as MST-B). Note that the above formulas along with others [21] can only be used for temperatures up to 4 MeV. As stated earlier, many attempts to look for the temperature of the fragments exist in the literature. The value of the temperature depends on the reaction and situation. Generally, the limiting temperature fluctuates around 4 MeV (3–6 MeV) and depends on the method of extraction [10,17–19]. A smaller value of the temperature will yield larger differences in the binding energies, whereas this difference will diminish with temperature. For higher temperature, there should be no effect in the relative yields. Since the present binding energy formula is for temperature up to 4 MeV, we concentrate our present discussion on $T = 4$ MeV (labeled as MST-BT). All fragments are now subjected to the above binding energy checks.

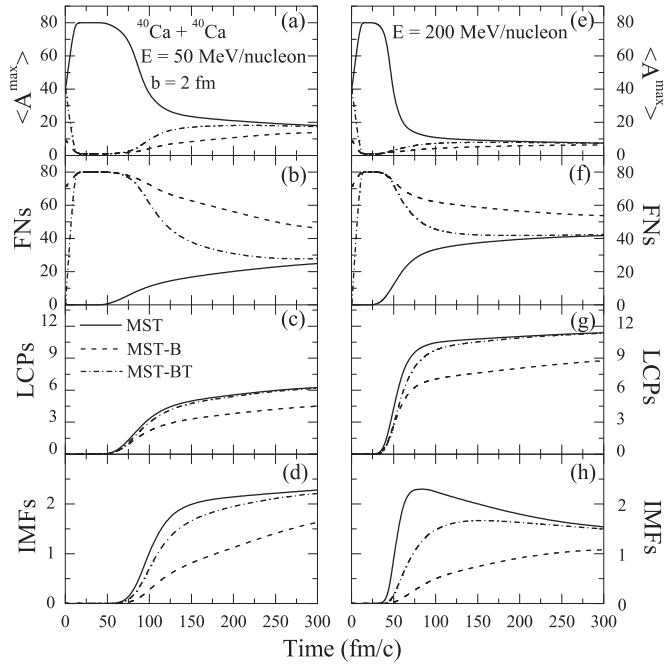

FIG. 1. The time evolution of different fragments for the reaction of ^{40}Ca + ^{40}Ca at 50 MeV/nucleon (left panels) and 200 MeV/nucleon (right panels) at an impact parameter of 2 fm. The results obtained with MST, MST-B, and MST-BT are shown.

III. RESULTS AND DISCUSSION

For the present analysis, we simulated the reactions of ^{40}Ca + ^{40}Ca and ^{197}Au + ^{197}Au at incident energies of 50 and 200 MeV/nucleon and over the full impact parameter range between 0 and $b_{\max}$ ($= R_P + R_T$, where R_P is radius of the projectile and R_T is the radius of the target) using a soft equation of state along with an energy-dependent nucleon-nucleon cross section. The reactions are simulated till 300 fm/c. This choice covers the entire system size, incident energies, and colliding geometry dependence.

In Fig. 1, we display the time evolution of the heaviest fragment ($\langle A^{\max}\rangle$), free nucleons (FNs), light charged particles (LCPs) [$2 \leqslant A \leqslant 4$], and intermediate mass fragments (IMFs) [$5 \leqslant A \leqslant A/3$] for the semicentral collisions ($b = 2$ fm) of ^{40}Ca + ^{40}Ca at 50 MeV/nucleon (left panels) and 200 MeV/nucleon (right panels). The solid, dashed, and dash-dotted lines correspond to MST, MST-B, and MST-BT methods, respectively. As noted, $\langle A^{\max}\rangle$ in the MST method increases initially and reaches a maximal point during the highly dense phase. The excitation energy stored in the system during the collision causes this single big fragment to decay into free nucleons, LCPs, and IMFs at the later stage of the reaction. Moreover, at the freeze-out stage, the size of $\langle A^{\max}\rangle$ is small at higher incident energy because of the violent nature of the reaction. When one imposes cold binding energy (MST-B), one finds that the $\langle A^{\max}\rangle$ predicted using the MST method is not properly bound during the highly dense phase, so it makes all those nucleons free. As noted in a previous study [15], when the binding energy of cold matter is implemented, one gets the (false) impression that the structure obtained in the MST method is not properly bound since there is a significant deviation in the MSTB results compared to those from the MST method. The size of heaviest fragment, LCPs, and IMFs (all bound structures) are fewer in the MST-B method compared to the MST method, indicating that the fragments created in the MST method are not properly bound and therefore are more likely to appear as a group of free nucleons rather than a bound fragment.

Note that, on an average, thermal binding energies at 4 MeV are about 25% less than the corresponding cold binding energies. In other words, while using the cold binding energies, we subject fragments to a binding energy check which is much more stringent than in reality. As a result, one finds fewer bound structures in terms of $\langle A^{\max}\rangle$, LCPs, IMFs (and other masses not shown here). Once thermal binding energies are implemented, we are close to reality and we now see that (i) the fragment structure can be identified much earlier (as early as 100–150 fm/c) and (ii) there are many more bound structures in the form of $\langle A^{\max}\rangle$, LCPs, IMFs, etc. [which occurs because now we demand lower binding energies (close to the realistic one)], (iii) there is a significant effect of thermal (temperature-dependent) binding energy on the fragment structure, and (iv) very interestingly, the results after the thermal binding energies cut agree very well with the results obtained with the normal MST method. This is a very important result since it validates the use of the MST method in studying fragmentation in heavy-ion reactions. It also refutes the fear that the MST method may not yield proper bound structures.

In Figs. 2 and 3, we display the size of the heaviest fragment and the multiplicities of FNs, LCPs, and IMFs as a function of impact parameter for the reactions of ^{40}Ca + ^{40}Ca

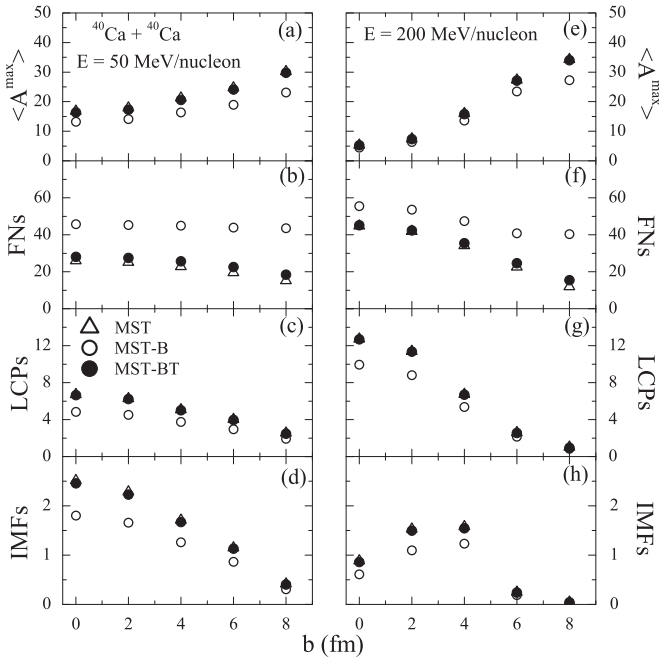

FIG. 2. The impact parameter dependence of the size of the heaviest fragment $\langle A^{\max}\rangle$ and the multiplicities of free nucleons, LCPs, and IMFs for the reaction of ^{40}Ca + ^{40}Ca at 50 MeV/nucleon (left panels) and 200 MeV/nucleon (right). The triangles and open and solid circles represent the results of MST, MST-B, and MST-BT, respectively.

and ^{197}Au + ^{197}Au at 50 MeV/nucleon (left panels) and 200 MeV/nucleon (right panels), respectively. The solid (open) circles represent the results using the MST-BT (MST-B) method whereas triangles correspond to the normal MST calculations. From the figures, we find that the size of the

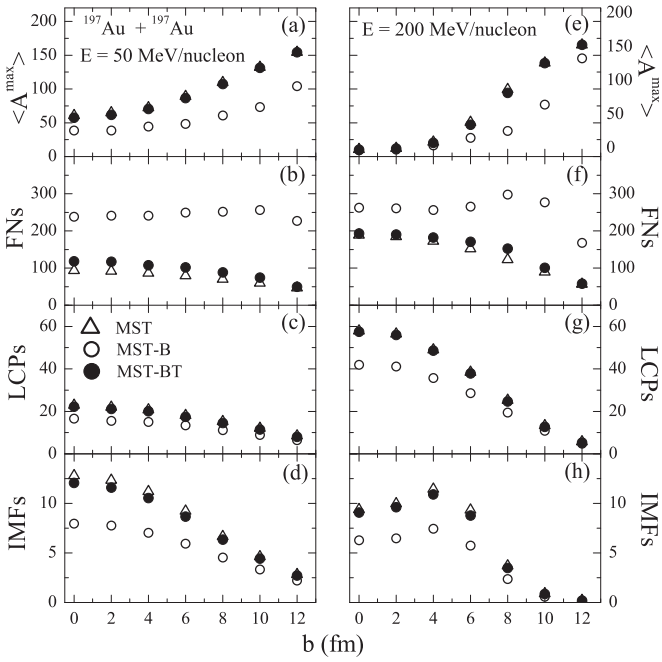

FIG. 3. Same as Fig. 2, but for the reactions of ^{197}Au + ^{197}Au at 50 MeV/nucleon (left panels) and 200 MeV/nucleon (right panels).

heaviest fragment (free nucleons) increases (decreases) when we go from central to peripheral collisions. This is because of the less violent nature of the collisions at peripheral geometries and thus both the projectile and target remain almost intact yielding bigger $\langle A^{\max}\rangle$. Similarly, the multiplicities of the LCPs and IMFs decrease for peripheral collisions except for the IMF multiplicity at 200 MeV/nucleon (lower right panel) where a rise and fall behavior is observed. Similar results were also reported earlier [3]. We also notice that the multiplicity is higher using a thermal binding energy check compared to the cold one. The point mentioned in Fig. 1 regarding the significant effect of the thermal treatment of binding energy remains valid at all incident energies as well as impact parameters.

In Fig. 4, we display the rapidity distributions of the free nucleons (top panels), LCPs (middle), and IMFs (bottom) for the reactions of ^{40}Ca + ^{40}Ca (left panels) and ^{197}Au + ^{197}Au (right) at incident energy of 50 MeV/nucleon. We define the rapidity of the ith particle as

$$Y(i) = \frac{1}{2}\ln\frac{\vec{E}(i) + \vec{p}_z(i)}{\vec{E}(i) - \vec{p}_z(i)}, \tag{11}$$

where $\vec{E}(i)$ and $\vec{p}_z(i)$ are the total energy and longitudinal momentum of the ith particle. The results displayed are at the freeze-out stage (300 fm/c). The lines have the same meaning

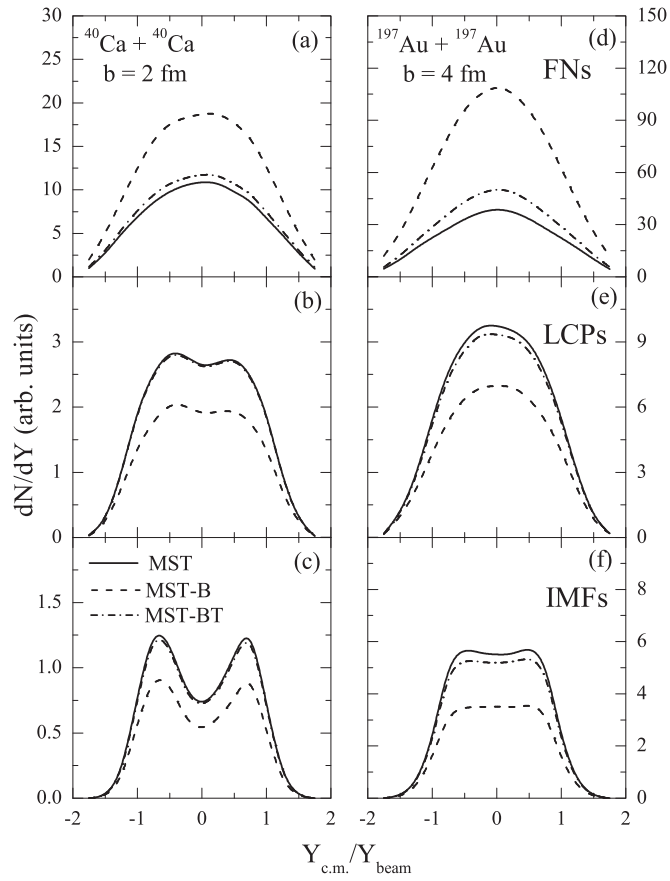

FIG. 4. The rapidity distributions (dN/dY) of free nucleons (top panels), LCPs (middle panels), and IMFs (bottom panels) at freeze-out time (300 fm/c) for the reactions of ^{40}Ca + ^{40}Ca (left panels) and ^{197}Au + ^{197}Au (right panels) at an incident energy of 50 MeV/nucleon. Lines have the same meaning as in Fig. 1.

as in Fig. 1. From the figure, we find that the rapidity distributions of the free nucleons and LCPs are maximum at mid rapidity, indicating their origin from the participant matter, whereas for the IMFs, the peak is at target and projectile rapidity, since they originate from the spectator matter. We also find that the fragment rapidity distribution using the normal MST and with a cold binding energy check ($T = 0$ MeV) shows a significant difference, as evident from earlier figures also. On the other hand, the rapidity distribution with thermal binding energies matches very well with that of the MST method. Again, a significant effect is seen in the rapidity distribution using thermal binding energies instead of cold binding energies.

To investigate the reason for the similar fragmentation pattern found using the normal MST method and the one with a thermal binding energy check, we look for the binding energies of the fragments formed in both methods: LCPs [$2 \leqslant A \leqslant 4$], medium mass fragments (MMFs) [$5 \leqslant A \leqslant 9$], heavy mass fragments (HMFs) [$10 \leqslant A \leqslant 15$], and IMFs [$5 \leqslant A \leqslant 13$] in the reaction of ^{40}Ca + ^{40}Ca and LCPs [$2 \leqslant A \leqslant 4$], MMFs [$5 \leqslant A \leqslant 20$], HMFs [$21 \leqslant A \leqslant 65$], and IMFs [$5 \leqslant A \leqslant 65$] in the reaction of ^{197}Au + ^{197}Au. The results are displayed in Fig. 5, where the lines have the same meaning as in Fig. 1. From the figure, we find that, when we use the normal MST method, the binding energy of all the fragments is initially positive (during the highly dense phase), indicating their instability; then, as the reaction proceeds, it becomes negative and the fragments gain stability. The unstable fragments formed with the MST method are discarded when the binding energy check is implemented. We also notice that fragments are more stable with cold binding energies compared to that at finite temperature. This is expected since, at higher temperatures, matter is excited and

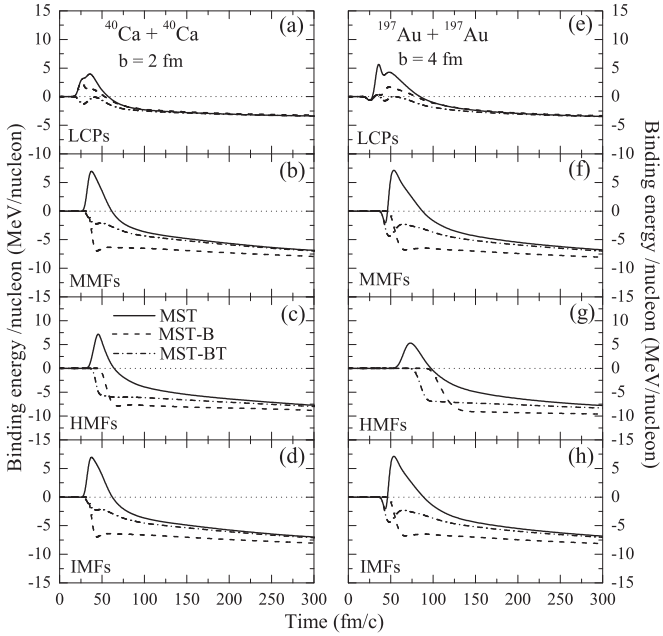

FIG. 5. The time evolution of the binding energy per nucleon of different fragments for the reactions of ^{40}Ca + ^{40}Ca (left panels) and ^{197}Au + ^{197}Au (right panels) at an incident energy of 200 MeV/nucleon. Lines have the same meaning as in Fig. 1.

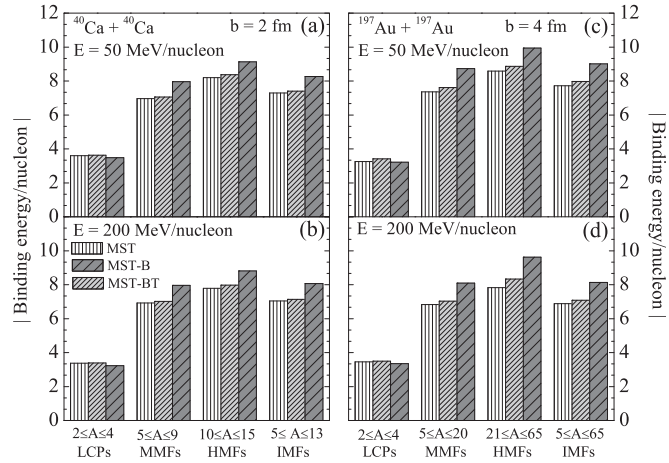

FIG. 6. The binding energies of LCPs, MMFs, HMFs, and IMFs formed in the reactions of ^{40}Ca + ^{40}Ca (left panels) and ^{197}Au + ^{197}Au (right panels) at 50 MeV/nucleon (top panels) and 200 MeV/nucleon (bottom panels) using MST, MST-B, and MST-BT methods.

less bound. We also find that light fragments (LCPs) are bound with about 3–4 MeV/nucleon whereas heavy fragments such as HMFs and IMFs have binding energy of 6–8 MeV/nucleon. This indicates that heavy fragments are more bound compared to lighter fragments. This is because the former originate from the spectator matter whereas latter are created during collisions from the participant matter, which is highly excited. It is worth noticing that, though at the freeze-out stage the binding energies obtained with the normal MST method match with that obtained using the thermal binding energy check at 4 MeV, one gets the stable bound configuration much earlier during a reaction with the latter (at around 50–70 fm/c) option.

In Fig. 6, we display the average binding energies of LCPs, MMFs, HMFs, and IMFs formed in the reactions of ^{40}Ca + ^{40}Ca (left panels) and ^{197}Au + ^{197}Au (right) at incident energies of 50 MeV/nucleon (upper panels) and 200 MeV/nucleon (lower panels). From the figure, we find that the binding energies of all fragments produced using the normal MST method as well as with the thermal binding energy check are almost the same whereas a significant difference can be seen from that of cold matter binding energies.

As far as stability of the fragments formed using the dynamical model (QMD+afterburners) is concerned, we have also studied the persistence coefficient of the fragments. The persistence coefficient provides information about the stability of the fragments between two successive time steps [11,22]. If a fragment does not emit any nucleon between two subsequent time steps, the persistence coefficient is unity. On the other hand, the persistence coefficient is zero if the fragment disintegrates completely. In Fig. 7, we display the persistence coefficient for the IMFs produced in the reactions of ^{40}Ca + ^{40}Ca at 2 fm at incident energies of 50 and 200 MeV/nucleon. From the figure, we find that the persistence coefficient is close to unity at freeze-out stages, thus indicating the formation of stable fragments. A slightly higher value of the persistence coefficient with MST-BT compared to that of MST-B indicates much stable fragments in the MST-BT method.

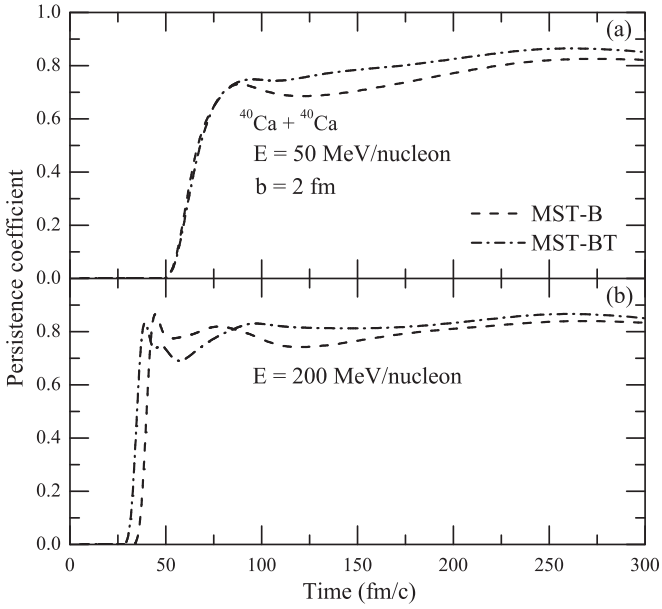

FIG. 7. The persistence coefficient of IMFs as a function of time in the reaction of ^{40}Ca + ^{40}Ca at an incident energy of 50 MeV/nucleon (upper panel) and 200 MeV/nucleon (lower panel).

In Fig. 8, we plot the transverse momentum (p_t) spectra of free nucleons, LCPs, and IMFs for the reactions of ^{40}Ca + ^{40}Ca (left panels) and ^{197}Au + ^{197}Au (right) at 50 MeV/nucleon. Again, the well-established trends seen in the previous pictures are also visible here.

As a last step, we compared our theoretical calculations using temperature-dependent binding energies with experimental data. As an example, we compare our results at low incident energy. A detailed comparison will be reported elsewhere [23]. Figure 9 shows the multiplicity of the fragments as a function of reduced impact parameter (b/b_{max}) for the reaction of ^{197}Au + ^{197}Au at an incident energy of 35 MeV/nucleon. The model predictions using MST-B and MST-BT approaches at the final stage are displayed along with experimental data taken with the combined Multics-Miniball (MM) array [24]. One can see a decreasing trend of the multiplicity with impact parameter. We also notice that our calculations with MST-BT are closer to the experimental measurements compared to that using MST-B.

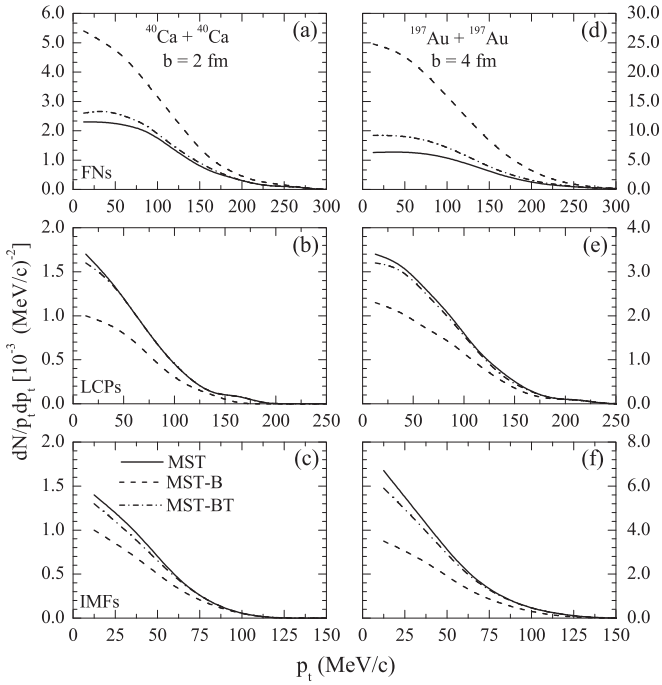

FIG. 8. $dN/p_t dp_t$ [(MeV/c)$^{-2}$] as a function of transverse energy p_t for free nucleons, LCPs, and IMFs for the reactions of ^{40}Ca + ^{40}Ca (left panels) and ^{197}Au + ^{197}Au (right panels) at an incident energy of 50 MeV/nucleon.

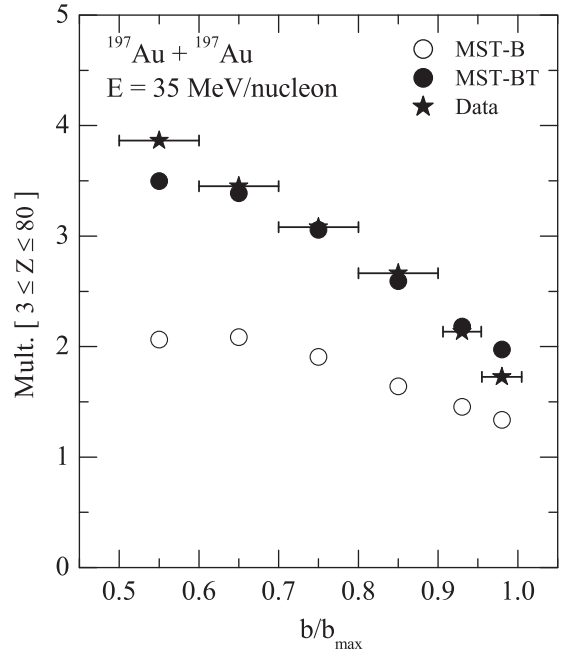

FIG. 9. The multiplicity of fragments [$3 \leqslant Z \leqslant 80$] as a function of reduced impact parameter for the reaction of ^{197}Au + ^{197}Au at an incident energy of 35 MeV/nucleon. The experimental data have been extracted from Ref. [24].

IV. SUMMARY

In this work, the minimum spanning tree method is improved by using thermal binding energies to validate the structure of the fragments. Our analysis for different masses, energies, as well as colliding geometries clearly indicates the significant role of the thermal binding energies over cold binding energies. The presented comparison with experimental measurements also signifies the importance of the use of thermal binding energies. The actual effect will depend on the temperature one is incorporating in the binding energies. Furthermore, our above thermal binding energy method can be used in any transport model.

ACKNOWLEDGMENT

This work is supported by Grant No. SR/FTP/PS-185/2012 from the Department of Science and Technology (DST), government of India awarded to S.G. under Young Scientist Scheme.

[1] B. Borderie and M. F. Rivet, Prog. Part. Nucl. Phys. **61**, 551 (2008); J. Pochodzalla *et al.*, Phys. Rev. Lett. **75**, 1040 (1995).
[2] G. F. Peaslee *et al.*, Phys. Rev. C **49**, R2271 (1994); R. Sun *et al.*, *ibid.* **61**, 061601(R) (2000).
[3] M. Begemann-Blaich *et al.*, Phys. Rev. C **48**, 610 (1993); M. B. Tsang *et al.*, Phys. Rev. Lett. **71**, 1502 (1993); A. Schüttauf *et al.*, Nucl. Phys. A **607**, 457 (1996).
[4] J. Singh, R. K. Puri, and J. Aichelin, Phys. Lett. B **519**, 46 (2001); J. Singh and R. K. Puri, Phys. Rev. C **65**, 024602 (2002).
[5] J. Aichelin, Phys. Rep. **202**, 233 (1991).
[6] W. Bauer, G. F. Bertsch, W. Cassing, and U. Mosel, Phys. Rev. C **34**, 2127 (1986).
[7] J. P. Bondorf *et al.*, Nucl. Phys. A **443**, 321 (1985); D. H. E. Gross, Rep. Prog. Phys. **53**, 605 (1990), and references therein; H. W. Barz *et al.*, Nucl. Phys. A **561**, 466 (1993).
[8] K. Hagel *et al.*, Phys. Rev. Lett. **68**, 2141 (1992); M. G. Mustafa, M. Blann, G. Peilert, and A. Botvina, Phys. Rev. C **49**, 2602 (1994).
[9] R. J. Charity *et al.*, Nucl. Phys. A **483**, 371 (1988); L. Wang *et al.*, *ibid.* **920**, 1 (2013).
[10] R. Wada *et al.*, Phys. Rev. C **55**, 227 (1997).
[11] C. Dorso and J. Randrup, Phys. Lett. B **301**, 328 (1993).
[12] R. K. Puri and J. Aichelin, J. Comput. Phys. **162**, 245 (2000); Y. K. Vermani *et al.*, J. Phys. G: Nucl. Part. Phys. **37**, 015105 (2010); Y. K. Vermani and R. K. Puri, Eur. Phys. Lett. **85**, 62001 (2009).
[13] S. Kumar and R. K. Puri, Phys. Rev. C **58**, 320 (1998); J. Singh and R. K. Puri, J. Phys. G: Nucl. Part. Phys. **27**, 2091 (2001).
[14] S. Kumar and R. K. Puri, Phys. Rev. C **58**, 2858 (1998).
[15] S. Goyal and R. K. Puri, Phys. Rev. C **83**, 047601 (2011).
[16] C. Samanta and S. Adhikari, Phys. Rev. C **65**, 037301 (2002); **69**, 049804 (2004).
[17] J. B. Natowitz *et al.*, Phys. Rev. C **65**, 034618 (2002).
[18] J. Wang *et al.*, Phys. Rev. C **72**, 024603 (2005).
[19] A. Barrañón, C. O. Dorso, and J. A. López, Nucl. Phys. A **791**, 222 (2007); L. Manduci *et al.*, *ibid.* **811**, 93 (2008).
[20] N. J. Davidson *et al.*, Phys. Lett. B **315**, 12 (1993); Nucl. Phys. A **570**, 61 (1994).
[21] C. Guet, E. Strumberger, and M. Brack, Phys. Lett. B **205**, 427 (1988); G. Sauer, H. Chandra, and U. Mosel, Nucl. Phys. A **264**, 221 (1976).
[22] C. O. Dorso and P. E. Balonga, Phys. Rev. C **50**, 991 (1994); C. Dorso and J. Aichelin, Phys. Lett. B **345**, 197 (1995).
[23] R. Kumar, S. Gautam, and R. K. Puri, Phys. Rev. C (to be published).
[24] M. D'Agostino and M. Bruno (private communication); Y. K. Vermani, Ph.D. thesis, Panjab University, Chandigarh, India, 2010.